Supporting Information

Seijffers et al. 10.1073/pnas.1314826111

SI Materials and Methods

Mouse Strains. All animal experiments were reviewed and approved by the Institutional Animal Care and Use Committee of Children's Hospital of Boston, University of Massachusetts Medical School, and Massachusetts General Hospital. This study used two activating transcription factor 3 (ATF3) transgenic mouse lines (19) (derived from two different founders) that constitutively express ATF3 in neurons, including spinal motor neurons, and were backcrossed at least seven generations into C57BL/6 mice. These mice were crossed with the high-copy number $SOD1^{G93A}$ transgenic mice (6) (stock number 002726; Jackson Laboratories). Mice progeny were distinguished by genotyping with specific primers for the human $SOD1^{G93A}$ mutant gene and primers specific for the ATF3 transgene. Progeny of four genotypes (WT, ATF3/WT, $SOD1^{G93A}$, and ATF3/$SOD1^{G93A}$) of matched littermates and gender was used unless otherwise indicated.

Evaluation of Disease Progression and Survival Rate. Disease onset, progression, and survival were monitored in the double transgenic ATF3/$SOD1^{G93A}$ compared with $SOD1^{G93A}$ mutant mice. All tests were performed blinded to the mouse genotype. The onset of the disease in the $SOD1^{G93A}$ mutant mice is at around 90 d of age; the disease progresses, and the mice die at ∼130–140 d. Examination of the mice began at ∼60 d of age. Mice were weighed and examined biweekly by lifting them up by their tails and viewing their hind limb flexibility, muscle tone, and weakness. At disease onset, the initial manifestation of weakness is a resting tremor of one limb (typically a hind limb). After onset was observed, mice were monitored daily for gait impairment and asymmetrical or symmetrical paralysis of the hind limbs. As the disease progresses, it eventually leads to death. Mice were euthanized when they were unable to right themselves within 15 s after being placed on their backs. All tests were performed blinded to the mouse genotype.

Grip Strength Analysis. Motor function/muscle strength was assayed biweekly beginning at 60 d of age using the grip strength test until the mice could no longer perform the task. The mice were trained to grip the bar of the grip strength apparatus (Chatillon) with their hind limbs, and then, they were pulled off the bar horizontally. Each measurement was performed in triplicate, and the force used to grip the bar was recorded in kilograms. All tests were performed blinded to the mouse genotype.

Motor Neuron Quantification. Mice were transcardiacly perfused with 4% (wt/vol) paraformaldehyde in phosphate buffer. The spinal cord lumbar region was excised and postfixed overnight in 4% (wt/vol) paraformaldehyde in phosphate buffer, and then, it was cryoprotected in 30% (wt/vol) sucrose in PBS; 10-μm-thick sections were double stained for the neuronal marker NeuN using a mouse monoclonal antibody at 1:2,000 dilution (Chemicon) and a rabbit polyclonal anti-ATF3 antibody at 1:200 (Santa Cruz) followed by cy3-conjugated goat anti-rabbit and FITC-conjugated goat anti-mouse secondary antibodies (Jackson ImmunoResearch). The ventral horn regions of eight nonadjacent sections (at least 600 μm apart per mouse) were used for the analysis. Motor neurons with clear cell body margins as detected by NeuN immunostaining with an area ≥ 450 μm^2 were quantified using Image J software. Only gender-matched littermates were used at 60, 90, and 120 d of age. For each group, three to four mouse litters were used, with a total of five mice per time point quantified.

Neuromuscular Junction Analysis. The gastrocnemius muscle was excised, postfixed in 4% (wt/vol) paraformaldehyde in PBS overnight, and cryoprotected in 30% (wt/vol) sucrose in PBS; 20-μm-thick sections were double stained with α-bungarotoxin 488 conjugate at 1:1,000 dilution (Molecular Probes) and rabbit anti-neurofilament 200 at 1:1,000 dilution (Sigma) followed by cy3 goat anti-rabbit antibody at 1:200 dilution (Jackson ImmunoResearch). All neuromuscular junctions with a pretzel-shaped morphology that stained positive for α-bungarotoxin binding to the acetylcholine receptor (AChR) were quantified on three nonadjacent sections at least 100 μm apart per mouse. Neuromuscular junctions were scored as innervated when both stains overlapped and scored as denervated when no neurofilament staining was detected. Gender-matched littermates were used; four to five litters per gender with a total of nine mice per group and time point were quantified at 60, 90, and 120 d of age. Terminal sprouts were determined when the nerve extended beyond the AChR clusters in any direction.

Ventral Root Counts. Mice were perfused transcardially with 4% (wt/vol) paraformaldehyde in phosphate buffer, and the L5 ventral roots were excised and postfixed in 2.5% (vol/vol) glutaraldehyde. The tissue was then treated with 1% osmium tetroxide for 1 h, dehydrated through graded alcohols, and embedded in Epon plastic (EM Sciences); 1-μm-thick cross-sections were cut on an ultramicrotome, stained with toluidine blue, rinsed, and coverslipped. Images were captured, and the axons' diameters were measured using the ImageJ software (National Institutes of Health). Three to four litters per gender with a total of six to nine mice per group per time point were quantified.

Statistical Analysis. One-way ANOVA was used to compare differences between groups over time. Kaplan–Meier log rank test for survival was used for comparing disease onset and lifespan between groups.

Microarray Analysis. Fresh frozen spinal cord lumbar region ventral horn samples of WT, ATF3/WT, $SOD1^{G93A}$, and ATF3/$SOD1^{G93A}$ at 90 d of age were subjected to RNA extraction using the TRIzol method (Invitrogen) with subsequent RNA cleanup and DNA digestion using the RNA Easy Micro Kit (Qiagen). RNA quality was tested using the 2100 Agilent Bioanalyzer (Agilent Technologies). The RNA was then reverse transcribed and labeled with biotin to generate biotin-labeled cRNA. Samples were then hybridized onto Illumina-Mouse WG6 v2.0 BeadChips. Arrays were then washed and stained with cy3-strepavidin and scanned in the Illumina BeadArray Reader. All 18 samples were processed at the same time under the same conditions. Each RNA sample used was extracted from one individual mouse. Five samples each were used for the $SOD1^{G93A}$ and ATF3/$SOD1^{G93A}$ mice, and four RNA samples each were used for the WT and ATF3/WT mice.

All analyses of expression were undertaken using the R programming environment (http://www.r-project.org). Probe summary profiles output by Illumina BeadStudio software after quantile normalization was read into R. Probes were retained for additional analysis only when the detection value was above 0.9 in at least two replicates from any of the tested conditions. Detection value was computed as one minus the detection *P* value characterizing the chance that the target sequence signal was distinguishable from the negative controls. Differential expression analysis was conducted by fitting a linear model to

18 microarrays and comparing the ATF3 transgenic genotypes with corresponding control using empirical Bayes moderated *t* statistics from the Bioconductor software package limma (59).

For gene ontology (GO) analysis, the likelihood of over-representation of GO categories in the up- or down-regulated genes relative to the background of all array genes was calculated using the National Institute of Health's DAVID Tool (Database for Annotation, Visualization, and Integrated Discovery), which implements a variant of Fisher exact test to test for enrichment of GO terms or Kyoto encyclopedia of genes and genomes (KEGG) pathways in a list of genes (60).

In the neuroinflammation category, several immune and inflammatory response pathways were detected by GO analysis. The pathways were scanned for redundancy and then combined into one heat map termed neuroinflammation. The pathways combined are GO:0006955~immune response, GO:0006954~inflammatory response, GO:0006952~defense response, GO:0002443~leukocyte-mediated immunity, GO:0045087~innate immune response, GO:0002460~adaptive immune response based on somatic recombination of immune receptors built from Ig superfamily domains, GO:0002250~adaptive immune response, GO:0002252~immune effector process, GO:0002253~activation of immune response, GO:0002449~lymphocyte-mediated immunity, GO:0050778~positive regulation of immune response, GO:0002274~myeloid leukocyte activation, GO:0019724~B cell-mediated immunity, GO:0050766~positive regulation of phagocytosis, GO:0002526~acute inflammatory response, GO:0045321~leukocyte activation, GO:0050764~regulation of phagocytosis, GO:0002684~positive regulation of immune system process, GO:0006909~phagocytosis, GO:0016064~Ig-mediated immune response, GO:0001817~regulation of cytokine production, GO:0045576~mast cell activation, GO:0006958~complement activation classical pathway, GO:0031349~positive regulation of defense response, GO:0045088~regulation of innate immune response, GO:0001819~positive regulation of cytokine production, GO:0002757~immune response-activating signal transduction, GO:0002455~humoral immune response mediated by circulating Ig, GO:0002695~negative regulation of leukocyte activation, GO:0050727~regulation of inflammatory response, GO:0051250~negative regulation of lymphocyte activation, GO:0002703~regulation of leukocyte-mediated immunity, GO:0006959~humoral immune response, GO:0042110~T-cell activation, GO:0002864~regulation of acute inflammatory response to antigenic stimulus, GO:0001816~cytokine production, GO:0046649~lymphocyte activation, GO:0002706~regulation of lymphocyte-mediated immunity, GO:0002694~regulation of leukocyte activation, GO:0032945~negative regulation of mononuclear cell proliferation, GO:0002819~regulation of adaptive immune response, GO:0002822~regulation of adaptive immune response based on somatic recombination of immune receptors built from Ig superfamily domains, and GO:0042116~macrophage activation.

The Gene Set Enrichment Analysis (GSEA) (46) was implemented to effectively evaluate the effect of a specific experimental condition on known biological pathways and functional categories. The GSEA analysis was performed with GSEA v2.0 software (http://www.broad.mit.edu/gsea/software/software_index.html). Briefly, ranked expression lists were derived based on limma B score when the experimental conditions in question were compared with its corresponding control. An enrichment score is then calculated for an a priori gene list or gene set that is associated with a particular molecular classification. In this study, analysis was performed against the entire GSEA database (MSigDB September 2010; http://www.broadinstitute.org/gsea/msigdb/index.jsp) after filtering out gene sets smaller than 15 and larger than 500 genes (as recommended); 4,000 permutations were performed for each sample set. Finally, the enrichment scores are normalized to account for differences in gene set size, and false discovery rate (FDR) is then calculated relative to the normalized enrichment score values to determine the false-positive rate. Gene sets with significant FDR and *P* value were submitted to a leading edge analysis. Significant FDRs and *P* values were less than 25% and 0.001, respectively, in accordance with GSEA recommendations. Leading edge analysis extracts the genes that contributed most significantly to the enrichment score.

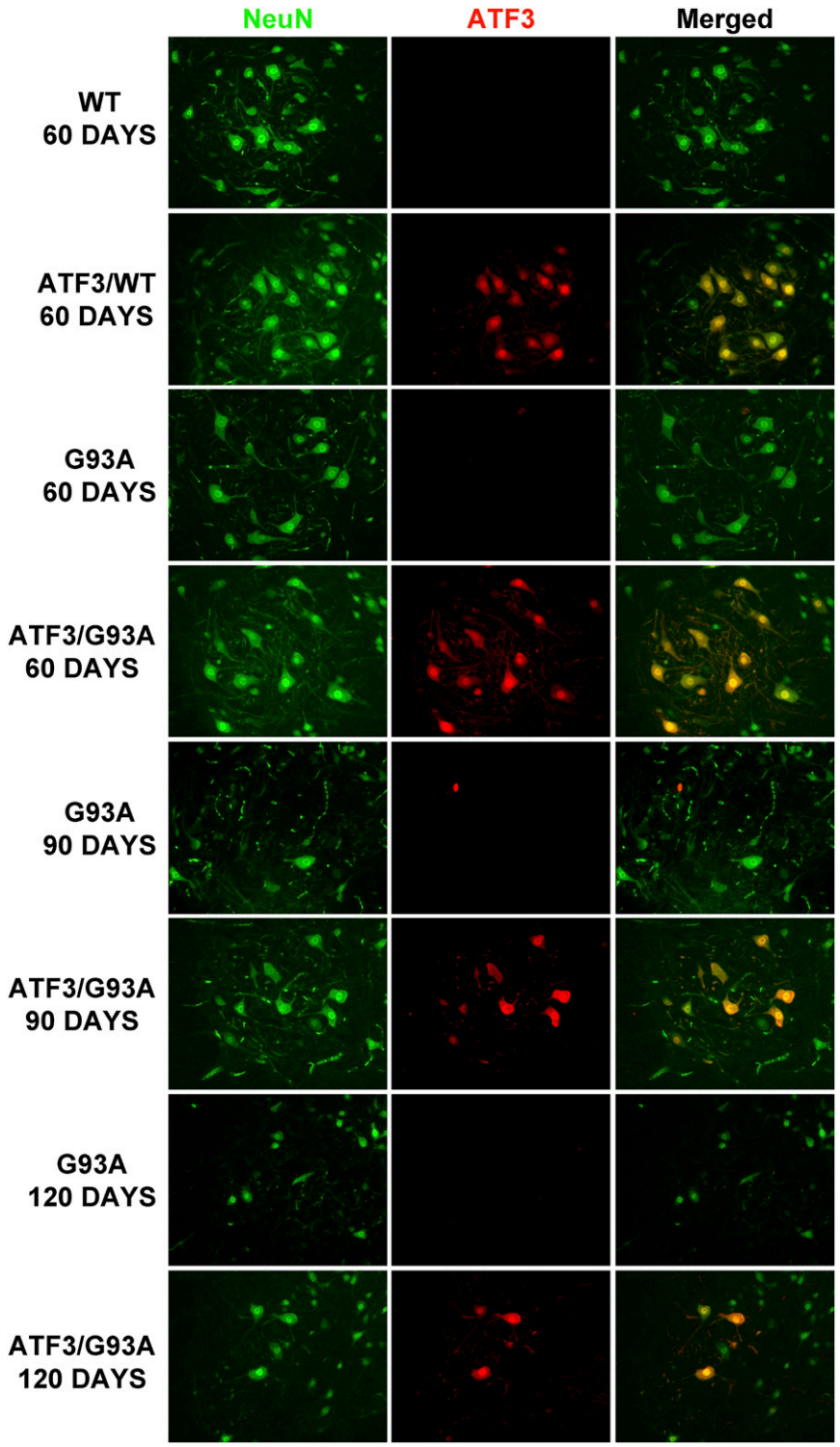

Fig. S1. ATF3 and NeuN immunostaining in the ventral horn of $SOD1^{G93A}$ and $ATF3/SOD1^{G93A}$ mice. Green, NeuN staining; red, ATF3 staining.

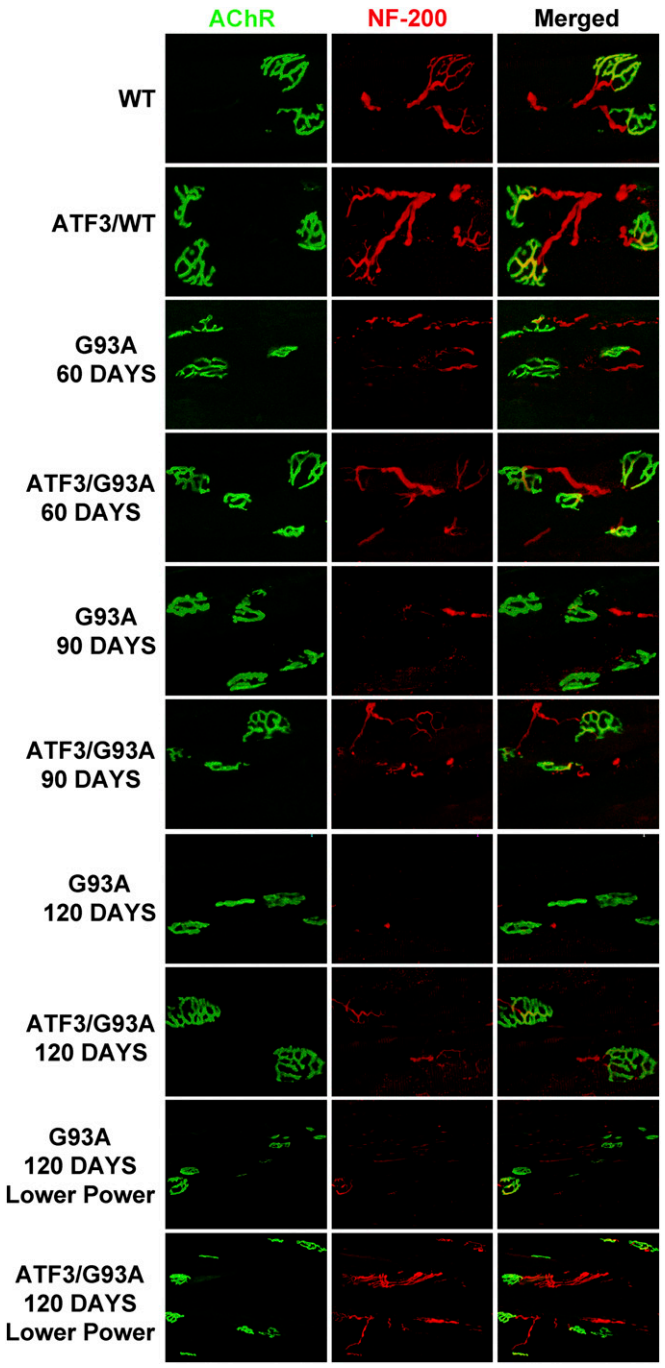

Fig. S2. Acetylcholine receptors and neurofilament double staining in the gastrocnemius muscle of $SOD1^{G93A}$ and $ATF3/SOD1^{G93A}$ mice. Green, α-bungarotoxin; red, neurofilament.

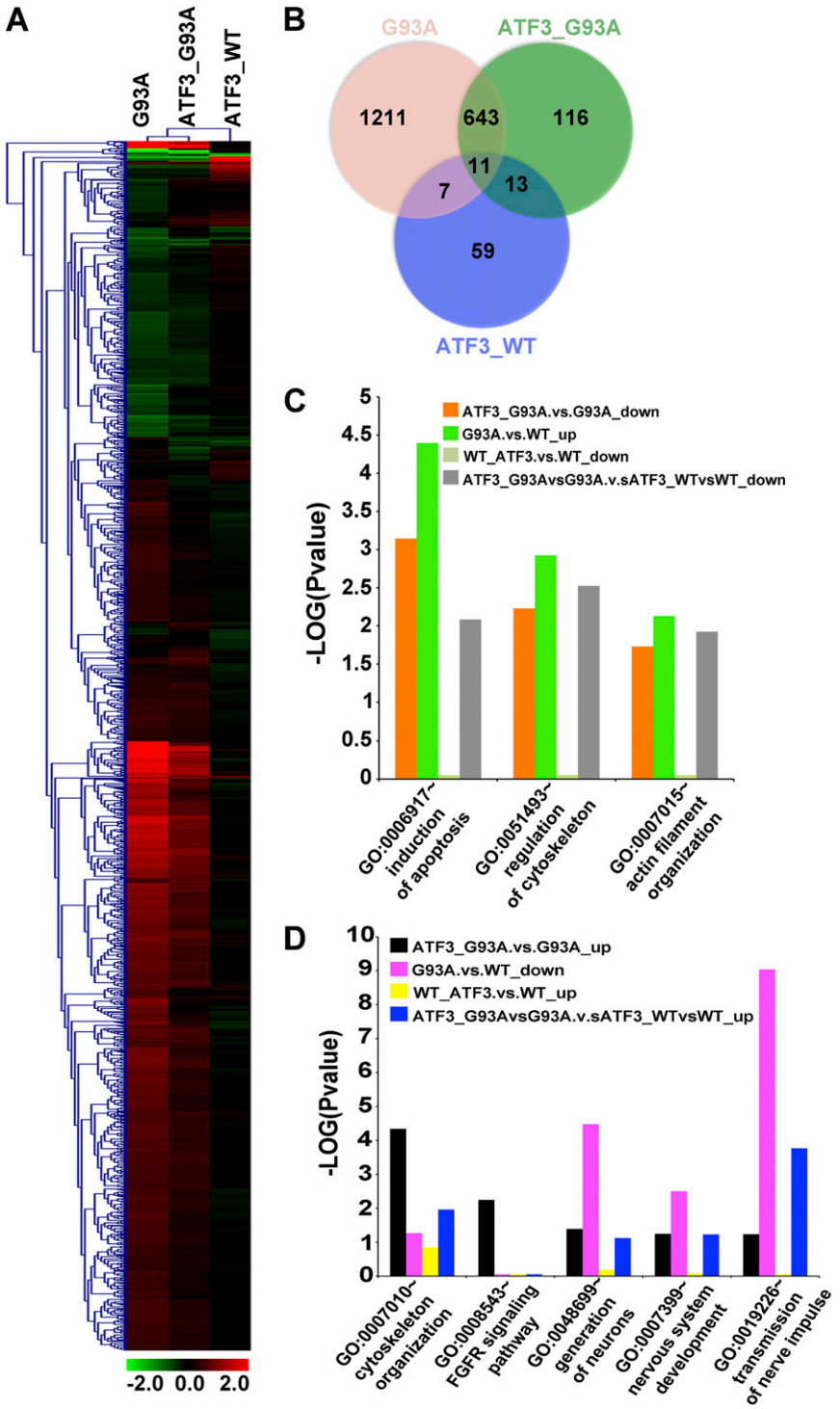

Fig. S3. Forced ATF3 expression in SOD1 mutant mice alters the transcriptome. (*A*) Microarray analysis was performed on ventral horn samples of 90-d-old SOD1^{G93A}, ATF3/SOD1^{G93A}, ATF3/WT, and WT mice, with $n = 5$ for SOD1^{G93A} and ATF3/SOD1^{G93A} samples and $n = 4$ for ATF3/WT and WT samples. A heat map for all genes in the dataset relative to WT mice with a minimum cutoff change fold of 1.2 and P value ≤ 0.05 comparing G93A, ATF3/G93A, and ATF3/WT is presented. (*B*) The Venn diagram illustrates the expression overlap of all sets of genes up- or down-regulated with a minimum cutoff change fold of 1.2 and P value ≤ 0.05 relative to WT. (*C*) Pathways that are significantly down-regulated in the ATF3/SOD1^{G93A} compared with the SOD1^{G93A} mice as identified by GO analysis. (*D*) Pathways significantly up-regulated in the ATF3/SOD1^{G93A} compared with the SOD1^{G93A} mice as identified by GO analysis. (*C* and *D*) _down represents a down-regulated pathway in each comparison, and _up represents an up-regulated pathway in each comparison. Significance is presented as −Log(P value), with a P value ≤ 0.05 [that is, a −Log(P value) ≥ 1.3] considered significant.

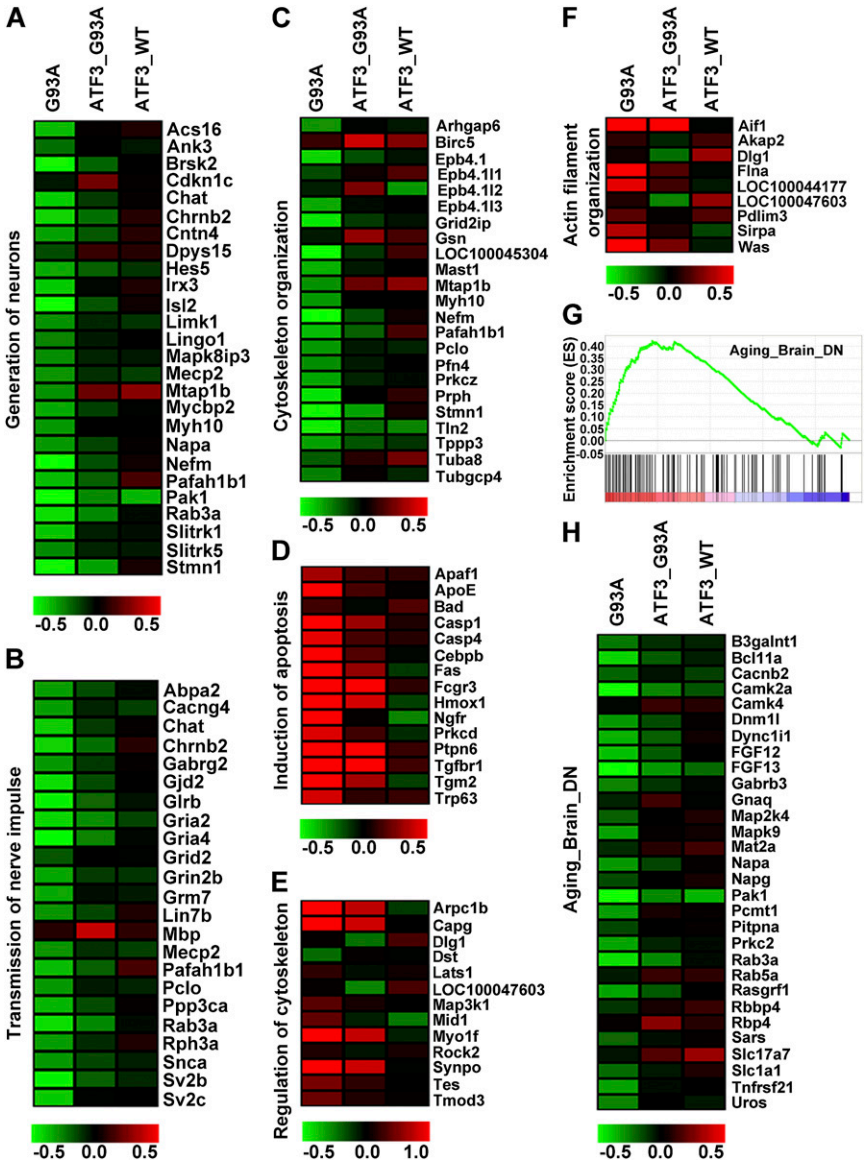

Fig. S4. Gene expression analysis reveals gene pathways involved in ATF3-mediated protection in ALS. (*A–F*) Heat maps showing the change fold difference in expression relative to WT for $SOD1^{G93A}$ (G93A), ATF3/$SOD1^{G93A}$ (ATF3/G93A), and ATF3/WT. [Scale bar: Log_2(change fold relative to WT).] Green, down-regulated; red, up-regulated. (*A*) GO:0048699~generation of neurons. (*B*) GO:0019226~transmission of nerve impulse. (*C*) GO:0007010~cytoskeleton organization. (*D*) GO:0006917~induction of apoptosis. (*E*) GO:0051493~regulation of cytoskeleton. (*F*) GO:0007015~actin filament organization. (*G*) GSEA analysis using MSigDB (molecular signature database) showed that genes that are down-regulated in the aging human brain are up-regulated in ATF3/G93A compared with G93A mice. Genes are ranked by signal-to-noise ratio according to their differential expression between ATF3/G93A and G93A. Genes in the gene set down-regulated in aging human brain are marked with vertical bars, and the enrichment score is shown in green. This gene set is highly modulated by ATF3, with a nominal P value ≤ 0.0001 and an FDR = 0.059. (*H*) Genes comprising the leading edge of the GSEA aging brain dataset are presented in a heat map. [Scale bar: Log_2(change fold relative to WT control).]

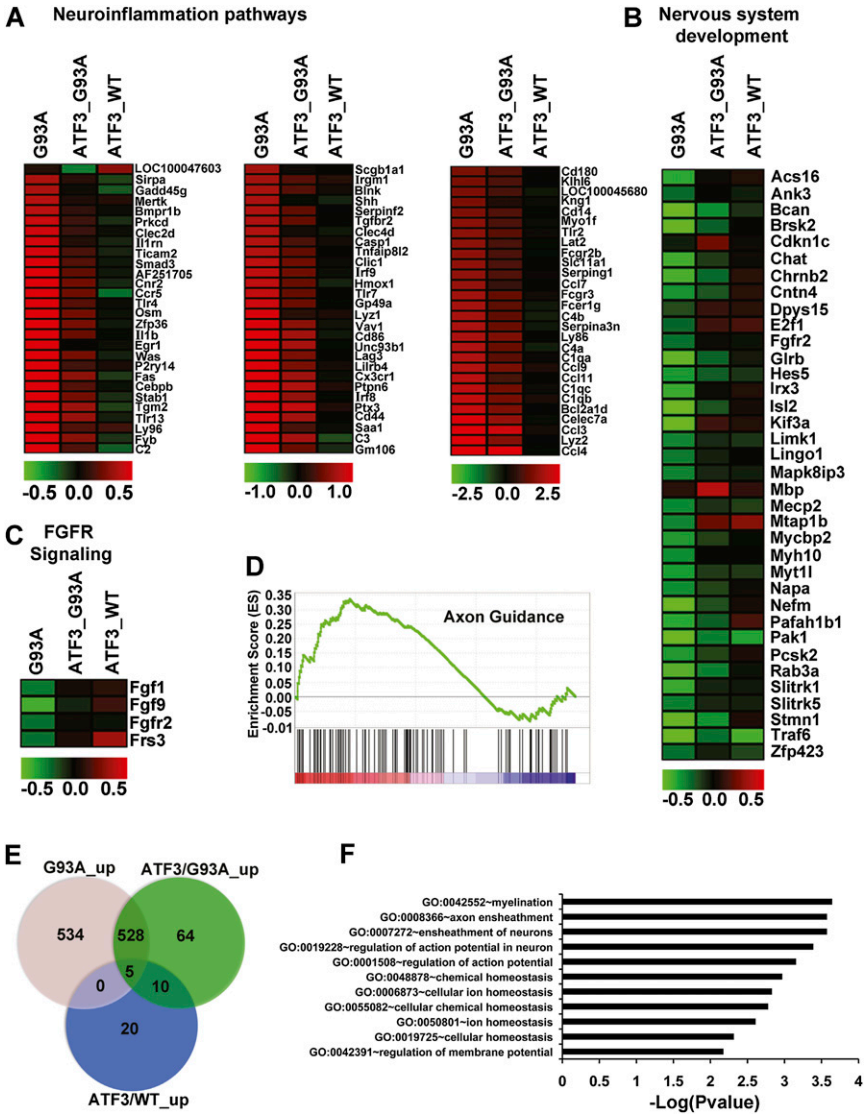

Fig. S5. Gene pathways involved in ATF3-mediated protection and pathways that are uniquely up-regulated in ATF3/SOD1^{G93A}. (*A*) Several immune and inflammatory response pathways detected by GO analysis were significantly down-regulated in ATF3/G93A compared with G93A mice. The pathways were scanned for redundancy and then combined into one heat map termed neuroinflammation (more information in *Materials and Methods*). Heat maps show the change fold difference in expression relative to WT for SOD1^{G93A} (G93A), ATF3/SOD1^{G93A} (ATF3/G93A), and ATF3/WT. [Scale bar: Log_2(change fold relative to WT).] Green, down-regulated; red, up-regulated. (*B*) GO:0007399~nervous system development. (*C*) GO:0008543~FGF receptor (FGFR) signaling pathway. (*D*) GSEA analysis detected a significant difference in the HSA04360 axon guidance pathway in ATF3/G93A compared with G93A, with a nominal *P* value of 0.0129 and FDR of 0.247. Genes in the leading edge include Ephb1, Chp, Dpysl5, Pak3, Sema5a, Sema5b, Nfat5, Limk1, Pak6, Epha6, Cfl2, Epna5, Rgs3, Efnb3, Srgap2, Dpysl2, Sema3a, Abl1, Pak1, Hras, Ppp3ca, Ppp3c, Cxcl12, Srgap3, Plxna2, L1cam, Sema6d, Ntng1, Epha4, Epha6, Unc5b, Ablim3, Sema4f, and Mapk3. (*E*) The Venn diagram illustrates the expression overlap of all sets of genes that are up-regulated, with a minimum cutoff change fold of 1.2 and *P* value $\leq$ 0.05 relative to WT. (*F*) Pathways identified by GO analysis in the set of 74 genes that are uniquely up-regulated in ATF3/SOD1^{G93A} compared with G93A. Significance is presented as −Log(*P* value), with a *P* value $\leq$ 0.05 [that is, a −Log(*P* value) $\geq$ 1.3] considered significant. No significant pathways were identified in the same category of uniquely down-regulated genes.

Movie S1. Limb motion in SOD1^{G93A} compared with ATF3/SOD1^{G93A} at 132 d of age. Gender- and age-matched SOD1^{G93A} and ATF3/SOD1^{G93A} littermates (females) are displayed. The SOD1^{G93A} littermate exhibits manifestations of paralysis, with visible decrease in limb motion, gait impairment, and dragging of rear quarters. In contrast, its ATF3/SOD1^{G93A} littermate preserves full range of motion.

Movie S1

Movie S2. End stage in the SOD1^{G93A} littermate. The same littermates shown in Movie S1 are presented at 137 d of age. The SOD1^{G93A} littermate reached end stage, whereas the ATF3/SOD1^{G93A} littermate is viable and only begun to display some limb motion impairment. This ATF3/SOD1^{G93A} littermate reached end stage 14 d later at 151 d of age.

Movie S2